1993

Ozone Observations and a Model of Marine Boundary Layer Photochemistry During SAGA 3

A. M. Thompson

J. E. Johnson

A. L. Torres

T. S. Bates

K. C. Kelly

See next page for additional authors

Citation/Publisher Attribution

Thompson, A. M., et al. (1993), Ozone observations and a model of marine boundary layer photochemistry during SAGA 3, *J. Geophys. Res.*, 98(D9), 16955–16968, doi: 10.1029/93JD00258.
Available at: https://doi.org/10.1029/93JD00258

JOURNAL OF GEOPHYSICAL RESEARCH, VOL. 98, NO. D9, PAGES 16,955–16,968, SEPTEMBER 20, 1993

Ozone Observations and a Model of Marine Boundary Layer Photochemistry During SAGA 3

A. M. THOMPSON,[1] J. E. JOHNSON,[2] A. L. TORRES,[3] T. S. BATES,[2] K. C. KELLY,[2] E. ATLAS,[4] J. P. GREENBERG,[4] N. M. DONAHUE,[5,6] S. A. YVON,[7] E. S. SALTZMAN,[7] B. G. HEIKES,[8] B. W. MOSHER,[9] A. A. SHASHKOV,[10] AND V. I. YEGOROV[11]

A major purpose of the third joint Soviet-American Gases and Aerosols (SAGA 3) oceanographic cruise was to examine remote tropical marine O_3 and photochemical cycles in detail. On leg 1, which took place between Hilo, Hawaii, and Pago-Pago, American Samoa, in February and March 1990, shipboard measurements were made of O_3, CO, CH_4, nonmethane hydrocarbons (NMHC), NO, dimethyl sulfide (DMS), H_2S, H_2O_2, organic peroxides, and total column O_3. Postcruise analysis was performed for alkyl nitrates and a second set of nonmethane hydrocarbons. A latitudinal gradient in O_3 was observed on SAGA 3, with O_3 north of the intertropical convergence zone (ITCZ) at 15–20 parts per billion by volume (ppbv) and less than 12 ppbv south of the ITCZ but never ≤3 ppbv as observed on some previous equatorial Pacific cruises (Piotrowicz et al., 1986; Johnson et al., 1990). Total column O_3 (230–250 Dobson units (DU)) measured from the *Akademik Korolev* was within 8% of the corresponding total ozone mapping spectrometer (TOMS) satellite observations and confirmed the equatorial Pacific as a low O_3 region. In terms of number of constituents measured, SAGA 3 may be the most photochemically complete at-sea experiment to date. A one-dimensional photochemical model gives a self-consistent picture of O_3-NO-CO-hydrocarbon interactions taking place during SAGA 3. At typical equatorial conditions, mean O_3 is 10 ppbv with a 10–15% diurnal variation and maximum near sunrise. Measurements of O_3, CO, CH_4, NMHC, and H_2O constrain model-calculated OH to 9×10^5 cm^{-3} for 10 ppbv O_3 at the equator. For DMS (300–400 parts per trillion by volume (pptv)) this OH abundance requires a sea-to-air flux of 6–8 $\times$ 10^9 cm^{-2} s^{-1}, which is within the uncertainty range of the flux deduced from SAGA 3 measurements of DMS in seawater (Bates et al., this issue). The concentrations of alkyl nitrates on SAGA 3 (5–15 pptv total alkyl nitrates) were up to 6 times higher than expected from currently accepted kinetics, suggesting a largely continental source for these species. However, maxima in isopropyl nitrate and bromoform near the equator (Atlas et al., this issue) as well as for nitric oxide (Torres and Thompson, this issue) may signify photochemical and biological sources of these species.

1. INTRODUCTION

The photochemistry of the equatorial Pacific boundary layer was first described by *Liu et al.* [1983] using data obtained on the R/V *Knorr 73/7* cruise (July to August 1978). Nitric oxide levels measured on that cruise averaged 4 parts per trillion by volume (pptv) during daylight hours and surface O_3 was ~10–15 parts per billion by volume (ppbv) [*McFarland et al.*, 1979]. On the *Knorr* cruise, NO in seawater was also measured and its supersaturation with respect to atmospheric NO was equivalent to a sea-to-air flux of ~10^8 cm^{-2} s^{-1} [*Zafiriou and McFarland*, 1981]; this is sufficient to explain the levels of atmospheric NO and HNO_3 observed on that cruise. *Thompson and Lenschow* [1984] demonstrated that these low NO levels, given the high moisture and solar insolation of the equatorial Pacific (with appreciable production of OH), are consistent with a diurnal cycle of O_3 increasing at night and decreasing during daytime. This diurnal pattern of surface O_3 has been confirmed on a number of oceanographic expeditions in the remote Pacific since the mid-1980s [*Piotrowicz et al.*, 1986, 1991; *Johnson et al.*, 1990].

The explanation for low O_3 in the equatorial Pacific is that O_3, supplied to the boundary layer by the stratosphere, undergoes photochemical destruction by UV photolysis and reaction with H_2O and is not replaced because concentrations of trace gases that lead to O_3 formation (NO_x and hydrocarbons) are very low. Evidence for this picture of remote marine chemistry has been collected through trace gas measurements on a number of oceanographic cruises. Examples include the 1980 R/V *Meteor* cruise [*Lowe and Schmidt*, 1982], the 1987 *Polarstern* cruise [*Rudolph and Johnen*, 1990; *Platt et al.*, 1992], and several NOAA/RITS (radiatively important trace species) cruises [see *Piotrowicz et al.*, 1986, 1991; *Johnson et al.*, 1990]. However, a comprehensive set of photochemically reactive trace gas measurements with sensitive instruments required for low concentrations has not been possible until recently. The third joint Soviet-American Gases and Aerosols oceanographic cruise (SAGA 3) on the R/V *Akademik Korolev* offered a platform to make a set of measurements with several state-of-the-art trace gas instruments and an opportunity to study

[1]NASA Goddard Space Flight Center, Greenbelt, Maryland.
[2]NOAA Pacific Marine Environmental Laboratory, Seattle, Washington.
[3]NASA Goddard Space Flight Center/Wallops Flight Facility, Wallops Island, Virginia.
[4]National Center for Atmospheric Research (NCAR), Boulder, Colorado.
[5]Massachusetts Institute of Technology, Cambridge.
[6]Now at Harvard University, Cambridge, Massachusetts.
[7]Rosenstiel School of Marine and Atmospheric Science, University of Miami, Miami, Florida.
[8]Graduate School of Oceanography, University of Rhode Island, Kingston.
[9]University of New Hampshire, Durham.
[10]Main Geophysical Observatory, St. Petersburg, Russia.
[11]Institute for Applied Physics, Laboratory for Atmospheric Monitoring, Moscow.

Paper number 93JD00258.
0148-0227/93/93JD-00258$05.00

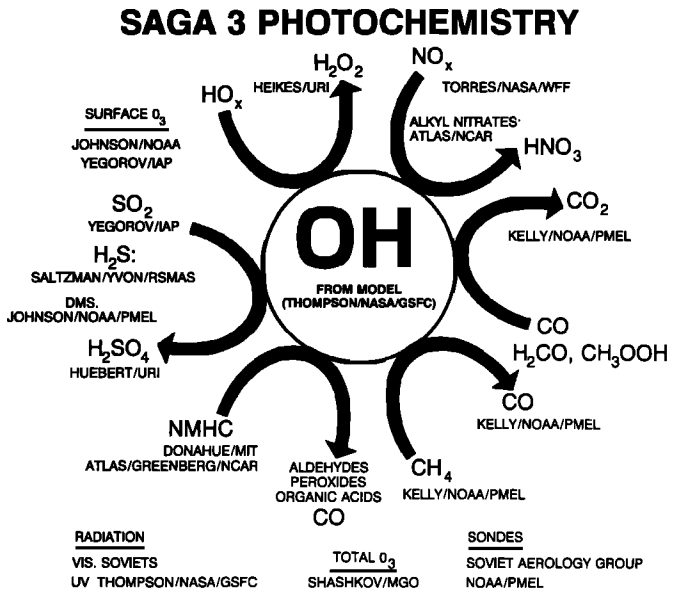

Fig. 1. Schematic illustration of the photochemical design of SAGA 3. Oxidation reactions that determine the loss rate of the OH radical are shown. The amount of UV (largely determined by total O_3), H_2O vapor, and ambient O_3 determine the rate of OH formation. Shipboard measurements of O_3, CO, CH_4, NO, nonmethane hydrocarbons, dimethyl sulfide (DMS), hydrogen peroxide (H_2O_2), organic peroxides, H_2S, UV, and visible radiation were made nearly continuously or at least several times per day. Radiosondes for pressure, temperature, and moisture were launched twice daily and a filter method was used to measure the total O_3 column on a dozen clear days. Grab samples collected on SAGA 3 gave samples for halocarbon analysis and a second set of nonmethane hydrocarbons; several dozen filter-trap extractions were analyzed post cruise for alkyl nitrates [*Atlas et al.*, this issue].

marine boundary layer O_3 and photochemical cycles of C-, N-, and S-containing gases in detail.

Figure 1 displays the photochemically reactive gases measured and the photochemical rationale on SAGA 3. Special emphasis was put on measuring the constituents required to constrain a model calculation of the hydroxyl radical. In this paper the O_3 data of SAGA 3 are presented along with a model synthesis of measurements of the photochemically reactive constituents. We attempt to answer the following questions:

1. Can a photochemical model reproduce typical SAGA 3 observations of O_3 and its precursors, CO, NO, CH_4, and nonmethane hydrocarbons in a self-consistent manner?

2. Can the diurnal behavior of O_3, NO, CO, and the peroxides observed on SAGA 3 be reproduced by a model? What do the observations imply about O_3 photochemical formation and about the NO_2/NO ratio, the so-called photostationary state?

3. Given that the model calculates OH (i.e., lifetimes) and sea-to-air fluxes of trace gases reacting with OH, how does the model-derived flux of dimethy sulfide (DMS) compare to that derived from SAGA 3 seawater DMS concentrations, assuming an air-sea gas exchange model with a transfer rate derived from observed winds [*Bates et al.*, this issue]? How does OH calculated by the one-dimensional NASA Goddard photochemical model compare with results from two box models used to evaluate SAGA 3 chemistry [*Donahue and Prinn*, this issue; *Yvon et al.*, this issue]?

The emphasis in the simulations presented in this paper is on mean SAGA 3 conditions and concentrations within 5° of the equator. However, to parameterize OH, calculations have also been performed for higher and lower O_3 levels observed on the cruise (20 ppbv O_3 at 10°N and 6 ppbv O_3 at 5°S). Several exceptional events occurred on SAGA 3; for example, chemical and meteorological conditions on Julian day 59 (February 28, 1990) were affected by a convective squall line [*Johnson et al.*, this issue].

Section 2 gives an experimental overview of the photochemical component of SAGA 3. Section 3 summarizes the trace gas measurements and describes the photochemical model. Section 4 discusses SAGA 3 O_3 observations. Model interpretation of SAGA 3 is given in section 5. First, O_3-CO-NO_x-hydrocarbon interactions are described, including an analysis of the O_3 and NO diurnal cycles. The peroxides and OH are reviewed and validation of the model for calculation of OH and deduction of the DMS sea-to-air flux is presented.

2. Experimental Overview of SAGA 3

2.1. *Trace Gas Measurements*

Figure 2 shows the cruise track of SAGA 3/leg 1, which took place from February 13, 1990 (Julian day 44), to March 13, 1990 (Julian day 72). The port of departure was Hilo, Hawaii, with the *Akademik Korolev* crossing the equator (and the intertropical convergence zone (ITCZ) 5 times en route to Pago-Pago, American Samoa). The purpose in multiple transects was to study interhemispheric gradients in greenhouse gases being measured on SAGA 3. However, there were gradients in a number of the photochemically reactive gases as well. Because the first north-to-south transect (along 145°W to 10°S) showed the ITCZ located 4°–6°N, subsequent transects were made between 5°S and 10°N (Figure 2).

Table 1 summarizes the major photochemical measurements on SAGA 3, including trace species or parameter measured, the instrument used, and the principal investigator with affiliation. Nine other SAGA 3 publications appear in this issue. The reader is referred to the following papers for experimental details and discussion of variability for

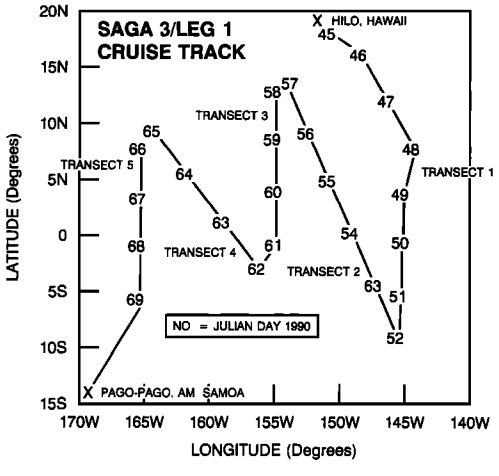

Fig. 2. Cruise track of SAGA 3/leg 1 from February 13, 1990 (Julian day 44), to March 13, 1990 (Julian day 72).

TABLE 1. Trace Gas Measurements on SAGA 3, Equatorial Pacific, February to March 1990

Species	Method	Investigator
O_3	Dasibi	J. Johnson (NOAA/PMEL) V. Yegorev (IAP/Moscow)
NO	chemiluminescence	A. Torres (GSFC/WFF)
Alkyl nitrates	charcoal traps, GC	E. Atlas (NCAR) A. Thompson (GSFC)
CH_4, CO	GC-FID CO—Hg bed detector	K. Kelly (NOAA/PMEL)
Nonmethane HC	shipboard GC	N. Donahue (MIT)
Nonmethane HC	flask, post-cruise GC	E. Atlas, J. Greenberg (NCAR) A. Thompson (GSFC)
H_2O_2, ROOH	peroxidase conversion and fluorescence	B. Heikes (URI), B. Mosher (UNH)
DMS	GC-ECD	J. Johnson (NOAA/PMEL)
H_2S	filter and extraction	S. Yvon, E. Saltzman (U. Miami)
SO_2	filter	V. Yegorev (IAP/Moscow)
O_3 column	M-83 filter	A. Shashkov and T. Kapustina (MGO/St. Petersburg, Russia)

species discussed in the present study: *Atlas et al.* [this issue], *Bates et al.* [this issue], *Donahue and Prinn* [this issue], *Huebert et al.* [this issue], *Johnson et al.* [this issue], *Torres and Thompson* [this issue], and *Yvon et al.* [this issue].

2.2. *Meteorological Data*

Figure 3 displays a summary of averaged temperature and humidity profiles from the twice daily sondes launched on the *Korolev*. The profiles illustrated are for those taken within 5° of the equator; daytime and nighttime profiles have been combined because there is little diurnal variation. Between 100 and 3000 m the day-night temperature difference was less than 1°. Temperature and humidity showed latitudinal gradients but little difference among transects. The mean boundary layer height is 1.5 km, with the greatest variation on isolated days during unusual meteorological episodes. Further details of SAGA-3 meteorology and trajectory analyses are given by *Johnson et al.* [this issue].

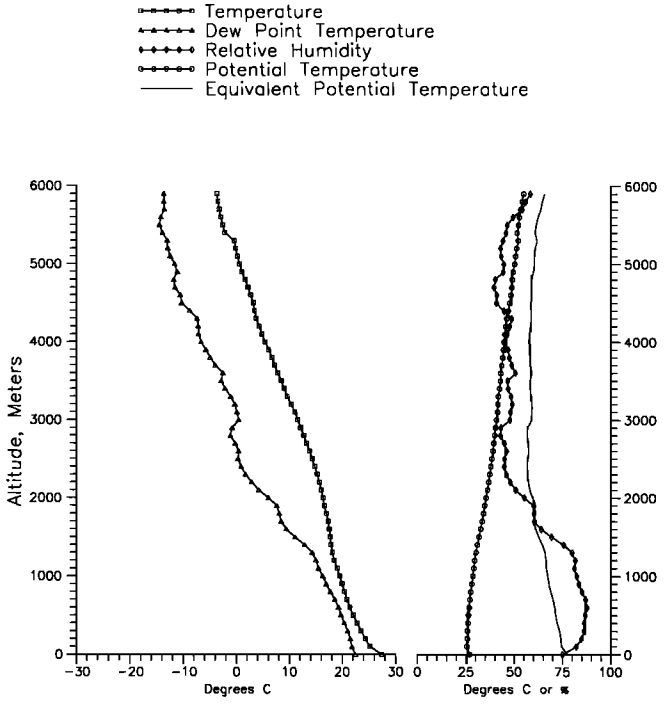

Fig. 3. Mean profiles of temperature and relative humidity from twice daily sondes launched from the *Akademik Korolev*. Average shown is from eight soundings made between 5°N and 5°S.

2.3. *Experimental Method for Ozone Measurements*

A Dasibi model 1008-AH O_3 photometer was used to measure O_3 concentrations. Ambient air at 1.5 L/min was sampled through a 90-m Teflon sampling line (inside diameter, 3 mm) that extended to the top of the starboard cargo crane mast. This length of Teflon tubing results in at most a 15% loss of O_3 [*Johnson et al.*, this issue]. The Dasibi photometer was calibrated relative to a (NIST) standard UV O_3 photometer. Over the range of ambient O_3 concentrations the uncertainty in the calibration of the Dasibi was approximately ± 3 ppbv reduced by time averages. The output analog voltage signal was digitized by a data logger and 1-min average values were recorded by a microcomputer system on floppy disks.

The zero level of the Dasibi was checked at 3-day intervals by first directing the sample air through a charcoal filter for a period of 1 hour. The zero level was reproducible to within a range of 0.8 ppbv. The zero level was subtracted and the O_3 data placed into 6-min averages. When these O_3 values were plotted, it was found that there were numerous electronic noise spikes of short duration. These were removed using the criteria that the natural variability of O_3 should be less than 3 ppbv per 6-min interval. After the data were cleaned, a time series of 1-hour averages was created.

3. PHOTOCHEMICAL MODEL CALCULATIONS

Both time-dependent and steady state versions of a one-dimensional photochemical model [*Thompson and Cicerone*, 1982; *Thompson et al.*, 1990] are used to simulate SAGA 3 trace gas data and to compute concentrations of transient species that cannot be measured. A one-dimensional model, strictly speaking, is valid only for one location and time and is best used for an air mass that is horizontally homogeneous. On SAGA 3 the one-dimensional model is assumed to be valid except for occasional deep convective episodes [*Johnson et al.*, this issue].

TABLE 2. Species and Boundary Conditions Used in SAGA 3 Model Simulations

Species	Upper Boundary, 15 km
O_3	stratospheric influx
$O(^3P)$	stratospheric influx
CH_3O_2, CH_3OOH, $C_2H_5O_2$	photochemical equilibrium
H_2O_2, C_2H_5OOH, CH_3CO_3, H, OH, HO_2	photochemical equilibrium
$NO_y(=NO + NO_2 + NO_3 + HNO_3 + HNO_4 + 2N_2O_5)$	stratospheric influx
H_2CO, PAN, CH_3CHO, C_3H_8, C_3H_6, C_2H_4	zero flux
CO, C_2H_6	troposphere-to-stratosphere transfer
$C_3H_6OHO_2$, CH_2O_2, $C_2H_4O_2$, 1-$C_3H_7O_2$, 2-$C_3H_7O_2$, $C_2H_4OHO_2$, $C_2H_5ONO_2$, 1-propyl nitrate, 2-propyl nitrate, SO_2, DMS, SO_3, COS, CS_2, HSO_3, H_2S	zero flux

Species	Lower Boundary, 0 km
O_3,$O(^3P)$	deposition
CH_3O_2, $C_2H_5O_2$, CH_3CO_3, $C_3H_6OHO_2$, CH_2O_2, $C_2H_4O_2$, $C_2H_4OHO_2$, 1-$C_3H_7O_2$, 2-$C_3H_7O_2$	photochemical equilibrium
H, OH, HO_2	photochemical equilibrium
NO	flux
NO_2, NO_3, N_2O_5, PAN	deposition
H_2CO, CH_3OOH, CH_3CHO, C_2H_5OOH	deposition
H_2O_2, HNO_3, HNO_4, $C_2H_5ONO_2$, 1-propyl nitrate, 2-propyl nitrate	deposition
C_2H_6, C_2H_4, C_3H_8, C_3H_6	flux
CO, H_2S, CS_2, COS, DMS	flux
SO_2, SO_3, HSO_3	deposition

Rainout with nonvarying first-order rate coefficient assumed for H_2O_2, HNO_3, H_2CO, HNO_4, PAN, CH_3CHO. For H_2 and CH_4, profiles are fixed; surface CH_4 constrained by observations [*Bates et al.*, this issue]. Transient species computed from photochemical equilibrium: HCO, $O(^1D)$, C_2H_5O, CH_3, CH_3O, C_3H_6OHO, $C_2H_4O_2^*$ and $CH_2O_2^*$ (Criegee intermediates), 1-C_3H_7O, 2-C_3H_7O.

The model vertical domain spans 0–15 km with 24 altitude grid points. Vertical transport is prescribed by eddy diffusion, as given by *Thompson and Cicerone* [1982]; eddy diffusion coefficients below 100 m define a distinct surface boundary layer [*Thompson and Lenschow*, 1984]. Temperature and water vapor up to 6 km are prescribed using the mean profiles in Figure 3 with climatology specified up to 15 km (U.S. Standard Atmosphere, 1966).

The model continuity equations are solved for 41 species (Table 2) and an additional 10 transients are computed from photochemical equilibrium. Profiles of CH_4 and H_2 are held constant; the CH_4 mixing ratio is fixed at the surface according to mean SAGA 3 observations [*Bates et al.*, this issue]. Boundary conditions include lower boundary fluxes for trace gases of oceanic origin (NO, hydrocarbons, CO, CS_2, DMS, H_2S, COS) and surface deposition for O_3, peroxides, SO_2, SO_3, all N-containing species except NO. Photochemical equilibrium boundary conditions are assumed for the remaining transients. At the upper boundary there is an assumed influx for O_3 and for odd nitrogen except for the alkyl nitrates. The nonmethane hydrocarbons (NMHC) selected for model simulation are chosen to represent the predominant lower alkanes and alkenes, C_2H_6, C_3H_8, C_2H_4, and C_3H_6, the oxidation of which contributes to aldehydes, organic peroxides, peroxyacetylnitrate (PAN), and CO. The formation and destruction of the ethyl, 1-propyl, and 2-propyl nitrates are also included; mechanisms and rate coefficients are given by *Roberts* [1990]. The model kinetics scheme for sulfur species, NMHC, and alkyl nitrates is given in Table 3.

Photodissociation rates are computed assuming clear sky conditions with an above-troposphere total O_3 column of 216 Dobson units (DU), which corresponds to 90% of the mean total O_3 measured by the Main Geophysical Observatory (MGO) instrument during the cruise period (Table 4). In other words, 10% of total ozone is assumed to be in the troposphere. The photodissociation rates are based on an equatorial solar flux for March 1, 1990.

Both steady state (diurnally averaged) and time-dependent model simulations are performed. The time-dependent version of the model is integrated until the 24-hour averages agree with those computed by the steady state calculation. Constituents with lifetimes of several weeks or more (O_3, CO, C_2H_6, PAN, alkyl nitrates) are slowest in reaching "steady state," i.e., a periodic 24-hour cycle. The time-dependent simulations are used to examine diurnal behavior of selected species. All mixing ratios given in summary tables are based on 24-hour averages or steady state model results in which "diurnally averaged" rate coefficients and photodissociation rates are used. Uncertainties in model-computed mixing ratios due to kinetics imprecisions can be estimated from uncertainties for an idealized marine tropical environment [*Thompson and Stewart*, 1991]. Some of the calculated imprecisions are greater than estimated instrumental precision, although at the concentrations of many species on SAGA 3, instrumental uncertainties as a fraction of mean mixing ratio can be appreciable (e.g., 15% for O_3, 20% for H_2O_2, and 35% for ROOH, the soluble hydroperoxides).

4. OZONE ON SAGA 3

The 1-hour averaged O_3 data are plotted as a function of latitude for each transect in Figure 4. The most obvious

TABLE 3. Model Rate Coefficients for Sulfur and Nonmethane Hydrocarbon Reactions

Reaction	Rate Coefficient
Photodissociation	
PAN + $h\nu \rightarrow CH_3CO_3 + NO_2$	
$C_2H_5ONO_2 + h\nu \rightarrow C_2H_5O + NO_2$	
*p*nitrate* + $h\nu \rightarrow NC_3H_7O + NO_2$	
*i*nitrate* + $h\nu \rightarrow IC_3H_7O + NO_2$	
Free radical	
$C_2H_6 + OH \rightarrow C_2H_5O_2 + H_2O$	$1.10E-11^* \exp(-1090./T)$
$C_2H_5O_2 + NO \rightarrow C_2H_5O + NO_2$	$4.20E-12^* \exp(180./T)$
$C_2H_5O + O_2 \rightarrow CH_3CHO + HO_2$	$1.20E-13^* \exp(-1350./T)$
$C_2H_5O_2 + HO_2 \rightarrow C_2H_5OOH + O_2$	$7.70E-14^* \exp(1300./T)$
$CH_3CHO + OH \rightarrow CH_3CO_3 + H_2O$	$6.87E-12^* \exp(255./T)$
$CH_3CO_3 + NO \rightarrow CH_3 + CO_2 + NO_2$	$2.38E-12$
$CH_3CO_3 + NO_2 + M \rightarrow PAN + M$	$5.49E-32$
$PAN + M \rightarrow CH_3CO_3 + NO_2 + M$	$3.18E-05^* \exp(-12500./T)$
$HO_2 + OH + M \rightarrow H_2O + O_2 + M$	
$CH_3O_2 + CH_3O_2 \rightarrow CH_3OH + H_2CO + O_2$	$1.00E-13^* \exp(220./T)$
$CH_3O_2 + CH_3O_2 \rightarrow CH_3O + H_2CO + O_2$	$6.80E-14^* \exp(220./T)$
$DMS + O \rightarrow SO_2$	$1.30E-11^* \exp(400./T)$
$DMS + OH \rightarrow SO_2$	$1.10E-11^* \exp(-240./T)$
$DMS + NO_3 \rightarrow SO_2 + NO_2$	$5.40E-13$
$SO_2 + O + M \rightarrow SO_3 + M$	*NASA/JPL* [1990]
$SO_2 + HO_2 \rightarrow SO_3 + OH$	$1.00E-18$
$SO_2 + OH + M \rightarrow HSO_3 + M$	*NASA/JPL* [1990]
$SO_3 + H_2O \rightarrow H_2SO4$	$9.10E-13$
$COS + O \rightarrow SO + CO$	$2.10E-11^* \exp(-2200./T)$
$COS + OH \rightarrow HS + CO_2$	$1.10E-13^* \exp(-1200./T)$
$CS_2 + O \rightarrow SO + CS$	$3.20E-11^* \exp(-650./T)$
$CS_2 + O \rightarrow COS + S$	$2.1E-37[M][T] \exp(2250./T)$
$CS_2 + OH \rightarrow COS + HS$	$8.80E-16^* \exp(2300./T)$
$HSO_3 + O_2 \rightarrow SO_3 + HO_2$	$1.30E-12^* \exp(-330./T)$
$HSO_3 + OH \rightarrow SO_3 + H_2O$	$1.00E-11$
$H_2S + O \rightarrow OH + HS$	$1.00E-11^* \exp(-1810./T)$
$H_2S + OH \rightarrow HS + H_2O$	$5.90E-12^* \exp(-65./T)$
$DMS + OH \rightarrow MSA$	$1.1E-12^* \exp(-240/T)$
$CH_3CHO + NO_3 \rightarrow CH_3CO_3 + HNO_3$	$1.40E-15$
$H_2CO + NO_3 \rightarrow HCO_3 + HNO_3$	$6.00E-16$
$C_3H_6 + OH \rightarrow C_3H_6OHO_2 + H_2O$	$4.10E-12^* \exp(537./T)$
$C_3H_6OHO_2 + NO \rightarrow C_3H_6OHO + NO_2$	$3.70E-12^* \exp(240./T)$
$C_3H_6OHO + M \rightarrow H_2CO + CH_3CHO$	$1.83E-16$
$C_3H_6OHO_2 + HO_2 \rightarrow C_3H_7O_3H + O_2$	$7.70E-14^* \exp(1300./T)$
$C_3H_6OHO_2 + CH_3O_2 \rightarrow CH_3O + C_3H_6OH + O_2$	$5.81E-14$
$C_3H_6 + O_3 \rightarrow CH_2O_2E + CH_3CHO$	$1.30E-14^* \exp(-2105./T)$
$CH_2O_2E^* + M \rightarrow CH_2O_2$	$1.72E-10$
$CH_2O_2E + M \rightarrow H_2 + CO_2$	$7.44E-11$
$CH_2O_2E + M \rightarrow H_2O + CO$	$1.28E-10$
$CH_2O_2E + M \rightarrow HCOOH$	$1.52E-11$
$CH_2O_2 + H_2O \rightarrow HCOOH + H_2O$	$4.00E-18$
$C_3H_6 + O_3 \rightarrow C_2H_4O_2E + H_2CO$	$1.30E-14^* \exp(-2105./T)$
$C_2H_4O_2E^* + M \rightarrow C_2H_4O_2$	$1.72E-10$
$C_2H_4O_2E + M \rightarrow CH_4 + CO_2$	$7.44E-11$
$C_2H_4O_2E + M \rightarrow CH_3OH + CO$	$1.28E-10$
$C_2H_4O_2E + M \rightarrow CH_3COOH$	$1.52E-11$
$C_2H_4O_2 + H_2O \rightarrow CH_3COOH$	$4.00E-18$
$C_3H_8 + OH \rightarrow NC_3H_7O_2 + H_2O$	$3.50E-12^* \exp(-750./T)$
$NC_3H_7O_2 + NO \rightarrow NC_3H_7O + NO_2$	$8.70E-12$
$NC_3H_7O + O_2 \rightarrow PALD$	$4.20E-13^* \exp(-2700./T)$
$NC_3H_7O_2 + HO_2 \rightarrow NC_3H_7OOH + O_2$	$7.70E-14^* \exp(1300./T)$
$NC_3H_7O_2 + CH_3O_2 \rightarrow NC_3H_7O + H_2CO + O_2$	$6.80E-14^* \exp(220./T)$
$NC_3H_7O_2 + NC_3H_7O_2 \rightarrow PALD + PALD + O_2$	$3.30E-13$
$IC_3H_7O + O_2 \rightarrow CH_3COCH_3$	$1.50E-14^* \exp(-200./T)$
$IC_3H_7O_2 + HO_2 \rightarrow IC_3H_7OOH + O_2$	$7.70E-14^* \exp(1300./T)$
$IC_3H_7O_2 + CH_3O_2 \rightarrow IC_3H_7O + H_2CO + O_2$	$5.81E-14$
$C_2H_5O_2 + NO \rightarrow C_2H_5ONO_2$	$4.20E-14^* \exp(280./T)$
$NC_3H_7O_2 + NO \rightarrow$ *p*nitrate	$1.70E-13$
$IC_3H_7O_2 + NO \rightarrow$ *i*nitrate	$3.80E-13$
$OH + C_2H_5ONO_2 \rightarrow PROD$	$4.80E-13$
OH + *p*nitrate → PROD	$7.00E-13$
OH + *i*nitrate → PROD	$1.80E-13$
$C_2H_4 + OH \rightarrow C_2H_4OHO_2 + H_2O$	$9.00E-12$
$C_2H_4OHO_2 + NO \rightarrow C_2H_4OHO + NO_2$	$3.70E-12^* \exp(240./T)$
$C_2H_4OHO_2 + HO_2 \rightarrow C_2H_4O_3H + O_2$	$7.70E-14^* \exp(1300./T)$
$C_2H_4OHO_2 + CH_3O_2 \rightarrow CH_3O + C_2H_4OH + O_2$	$5.81E-14$

Read $1.10E-11$ as 1.10×10^{-11}.

*Here *i*nitrate = 2-propylnitrate; *p*nitrate = 1 propylnitrate; $CH_2O_2E = C_4H_2O_2$*; $C_2H_4O_2E = C_2H_4O_2$*.

TABLE 4. Simulated and Observed Mixing Ratios

Species	Model, 24-hour Mean Mixing Ratio, 6.25 m	Observed Mixing Ratio [Reference]
O_3	9.3 ppbv	3–22 ppbv
NO	1.3 pptv	1.4 pptv, mean [*Torres and Thompson*, this issue]
NO_2	4.8 pptv	not measured
HNO_3	16 pptv	not measured
$RONO_2$, total	0.5 pptv	5–15 pptv [*Atlas et al.*, this issue]
CH_4	1.70 ppmv	1.7–1.8 ppmv, equator [*Bates et al.*, this issue]
CO	75 ppbv	60–80 ppbv [*Bates et al.*, this issue]
H_2O_2	590 pptv	580 pptv, mean
ROOH	610 pptv	640 pptv, mean
DMS	380 pptv	200–500 pptv [*Huebert et al.*, this issue]
H_2S	2.8 pptv	3 pptv, mean [*Yvon et al.*, this issue]
SO_2	53 pptv	2–50 pptv [*Yegorev*, 1990]
Nonmethane Hydrocarbons	Low, pptv	High, pptv	*Atlas et al.* [this issue] *Donahue and Prinn* [this issue]
C_2H_4	50	420	30–440 pptv
C_2H_6	790	790	500–1500 pptv
C_3H_6	55	150	30–400 pptv
C_3H_8	64	85	50–300 pptv

Model simulation based on above-tropospheric O_3 = 216 DU at equator for solar conditions of March 1, 1990.

feature is a north-south gradient, with nearly twice as much O_3 at the north extreme of each transect (usually 10°N) as at the south end (5° or 10°S). Although the north-south difference in O_3 mixing ratio is similar to what was seen on an April 1988 RITS cruise (170°W; *Johnson et al.* [1990]), the gradient on SAGA 3 is more gradual. This gradient also contrasts with equatorial data from two 1987 cruises reported by NOAA/PMEL (Pacific Marine Environmental Laboratory) [*Johnson et al.*, 1990]. A May 1987 cruise (SAGA 2, 160°–170°W) showed approximately equal O_3 mixing ratios in the bands at 0°–15°N and 0°–15°S and a July 1987 cruise (RITS 87, 155°–165°E) showed more O_3 in the southern hemisphere than in the northern hemisphere. The equatorial and southern hemisphere O_3 measurements on SAGA 3 compare well with O_3 observations at the NOAA/CMDL (Climate Monitoring and Diagnostics Laboratory) baseline monitoring station in American Samoa (14°S, 171°W). The O_3 seasonal cycle at Samoa, averaged over the period 1973–1984, shows a minimum mixing ratio in February of 8.3 ppbv and a July maximum of 19 ppbv [*Oltmans and Komhyr*, 1986].

A second feature of the SAGA data is low O_3 at the equator, although it is not so low as seen in some earlier expeditions [*Routhier et al.*, 1980; *Johnson et al.*, 1990]. This equatorial minimum is most pronounced for transect 1, with O_3 as low as 3–4 ppbv between 2° and 4°S. The minimum O_3 mixing ratio increases progressively with each more westerly transect, reaching 10 ppbv on transect 5 (Figure 4). Figure 4 shows a pronounced feature in the data on Julian day 59 (February 28, 1990). A peak in O_3 between 6° and 8°N on transect 3 coincided with the ship's passing through the wake of a mesoscale convective system, which brought down air with much lower than normal relative humidity. Nitric oxide measurements also increased during this episode. Mean daytime NO mixing ratios rose from 4–5 pptv to 10–20 pptv [*Torres and Thompson*, this issue], suggesting that drier air richer in NO and O_3 and originating above the boundary layer was mixed into the boundary layer during the episode of mesoscale descent. *Paluch et al.* [1992] report evidence for such behavior in eastern Pacific aircraft profiles of O_3, moisture, and potential temperature.

The low values of ozone seen at the surface on SAGA 3 are due not only to a scarcity of photochemical sources but also to low O_3 throughout the troposphere and stratosphere in the equatorial Pacific during the cruise. This is evident in Figure 5 which shows total column O_3 measured by a UV spectrophotometer aboard the *Akademik Korolev* (an M83-type filter instrument; *Gushchin et al.* [1976]) and total column O_3 measured by the Nimbus 7/TOMS (total ozone mapping spectrometer) for SAGA 3 dates and locations. Plate 1 shows a complete TOMS image for a representative day during February 1990 [*Shiotani*, 1992]. Total O_3 values are very low, in fact, the lowest total O_3 found outside of the Antarctic ozone hole. The "ground truth" afforded by the SAGA 3 data is unusual because surface measurements of total O_3 in the remote marine tropics are very limited. The TOMS-SAGA 3 M83 discrepancy, which ranges from 10 to 30 DU (4–11% of TOMS O_3), is probably within the accuracy of the M83 instrument (A. M. Shalamyanskiy, personal communication, 1991). However, the fact that TOMS measures higher total O_3 than the M83 is to be expected from the way the TOMS algorithm estimates the tropospheric contribution to total O_3 (R. D. McPeters, personal communication, 1992).

Piotrowicz et al. [1991] measured O_3 in the equatorial Pacific during the RITS 90 cruise aboard the R/V *Malcolm Baldridge* during January and February 1990. The RITS cruise was completing the westward part of its cruise track (from February 13 to 18, 1990, ending in Pago-Pago) as the *Korolev* was making its first southward transect from Hawaii. In general, the O_3 levels of RITS 90 and SAGA 3 were similar although the RITS data do not show an interhemispheric gradient because RITS was always south of the ITCZ. *Piotrowicz et al.* [1991] report three features of RITS that are similar to SAGA 3: (1) O_3 mixing ratios from 4 to 20 ppbv and typically ~10 ppbv; (2) one of two high O_3

episodes on RITS was associated with squall-line convection; (3) the low-O_3 regime extended across the entire mid-Pacific (Plate 1). *Piotrowicz et al.* [1991] propose that the large low-O_3 area is due to photochemical O_3 destruction combined with a weak Walker circulation bringing only small amounts of O_3-rich, stratospheric air to the boundary layer. A more detailed analysis of large-scale dynamics and equatorial O_3 is given by *Shiotani* [1992].

5. Results and Discussion

Average surface mixing ratios computed by the model are given in Table 4 along with the mean in situ trace gas measurements made on SAGA 3/leg 1. Concentrations are for "surface" level (5–15 m) and are reported as volume mixing ratios, except for the total ozone column (given in Dobson units, millimeter-atmosphere O_3).

5.1. *Ozone-NO-CO-HC Chemistry*

The diurnal cycle of O_3 (normalized as Del-O_3 ($O_3(t)$-diurnally averaged O_3), is shown in Figure 6, superimposed on O_3 measurements between 10°N and 10°S. Mean O_3 (9.3 ppbv) represents the "moderate" equatorial O_3 regime which characterized most of the cruise. The diurnal variation in SAGA 3 is not as pronounced as it was on previous equatorial Pacific cruises by the NOAA/PMEL group and is closest in behavior to the RITS 86 and SAGA 2 Indian Ocean transects of the equator [*Johnson et al.*, 1990]. The model results for SAGA 3 are qualitatively similar to the observations in showing a gradual O_3 increase during the night, a maximum near sunrise, and a decrease during the day. Ozone photochemistry is determined by destruction and formation processes as follows:

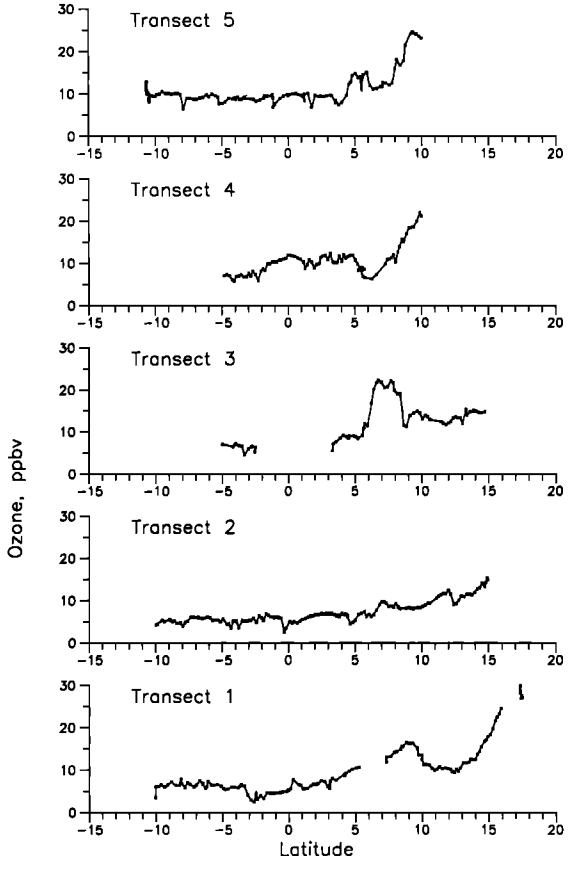

Fig. 4. Shipboard O_3 from the NOAA/PMEL (Pacific Marine Environmental Laboratory) Dasibi for the five north-south transects of SAGA 3. The IAP/LAM Dasibi data were identical when corrected by a slight offset in concentration from the NOAA/PMEL instrument. Gaps correspond to missing data from the PMEL instrument.

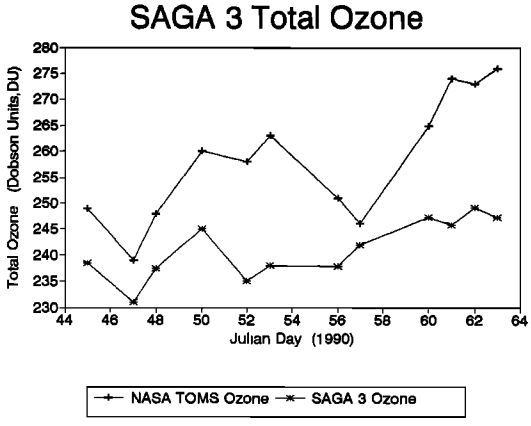

Fig. 5. Total column O_3 measured by the Main Geophysical Observatory (MGO) (St. Petersburg, Russia) M83 instrument aboard *Akademik Korolev*. NASA/TOMS (total ozone mapping spectrometer) total ozone for the same location and date are shown.

Destruction of O_3

$$O_3 + h\nu \rightarrow O(^1D) + O_2 \quad (1)$$

$$O(^1D) + H_2O \rightarrow OH + OH$$

Formation of HO_2 or RO_2 radicals

$$OH + CH_4 (+ O_2) \rightarrow CH_3O_2 + H_2O$$

$$OH + CO (+ O_2) \rightarrow CO_2 + HO_2$$

$$OH + RH (+ O_2) \rightarrow RO_2 + H_2O$$

Conversion of NO to NO_2

$$CH_3O_2 + NO \rightarrow NO_2 + CH_3O$$

$$HO_2 + NO \rightarrow NO_2 + OH$$

$$RO_2 + NO \rightarrow NO_2 + RO$$

Formation of O_3

$$NO_2 + h\nu \rightarrow O + NO$$

$$O + O_2 (+ M) \rightarrow O_3 + M$$

The reason for daytime O_3 loss in the equatorial Pacific is that levels of NO are so low that the NO to NO_2 conversion does not take place as rapidly as O_3 loss. Ozone losses during the day consist of UV photolysis (reaction (1)) and catalytic O_3 loss from OH and HO_2:

$$OH + O_3 \rightarrow HO_2 + O_2$$

$$HO_2 + O_3 \rightarrow HO + 2O_2$$

Ozone increases at night because the photochemical losses shut down. The photochemical model is used to compute the net rate of photochemical loss of O_3 over a daily

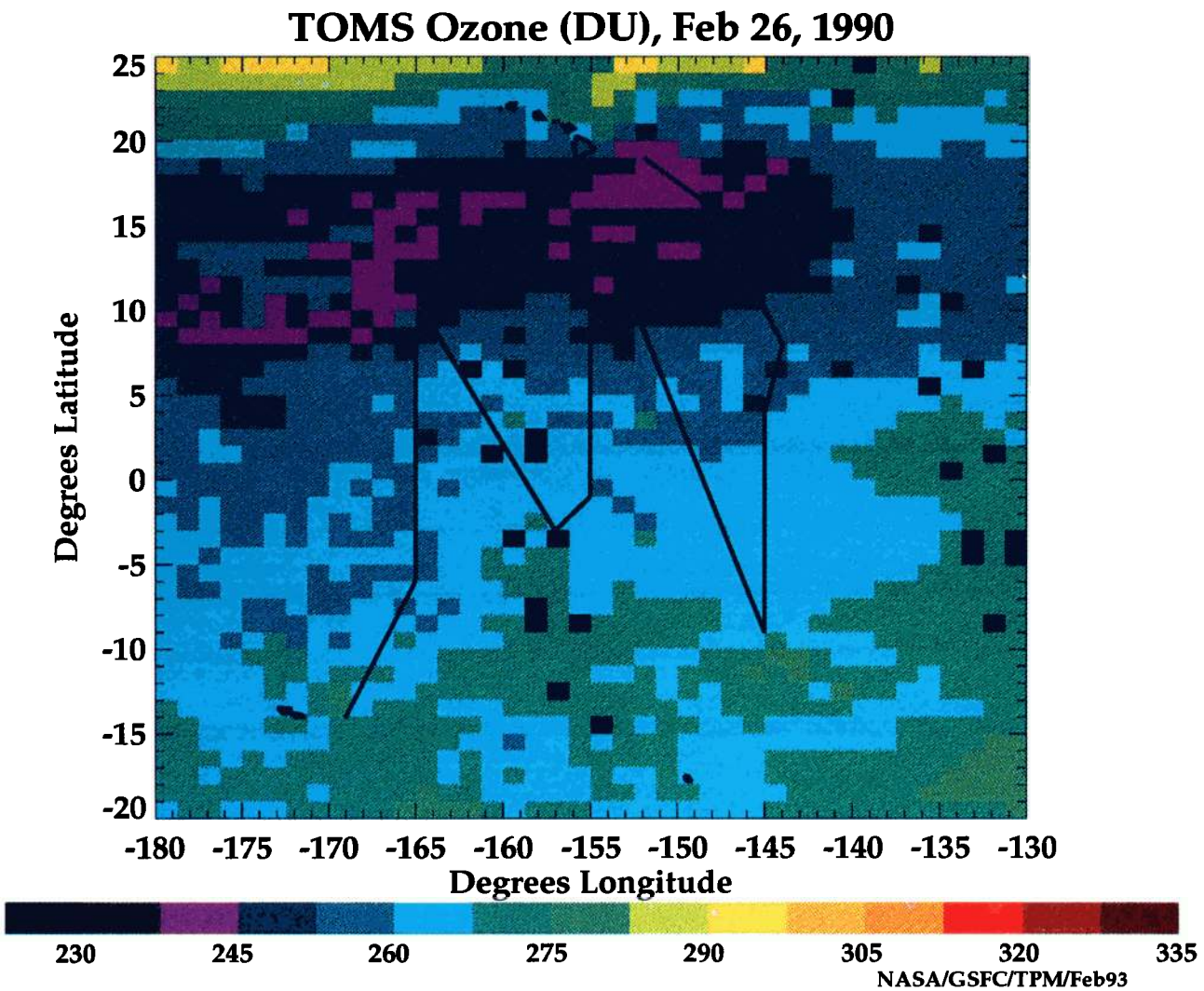

Plate 1. NASA TOMS satellite image from Nimbus 7 for a typical day during SAGA 3 (February 26, 1990). The low O_3 total column observed aboard the *Korolev* (Figure 5) is typical of the entire equatorial Pacific for this time of year [*Piotrowicz et al.*, 1991; *Shiotani*, 1992]. Cruise track is shown in black.

cycle by evaluating the difference between formation and destruction processes. The following expression, the so-called "ozone production potential" (OPP), is computed over a 1-day integration:

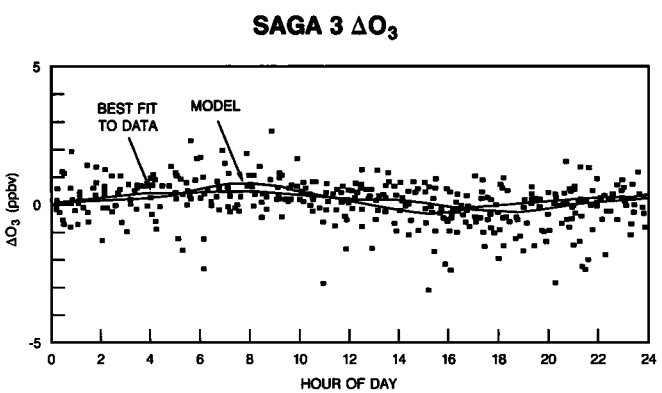

Fig. 6. Diurnal behavior of O_3 on SAGA 3 from measurements by the NOAA/PMEL instrument. The best fit to data and model-computed diurnal behavior of O_3, ($O_3(t)$-diurnally averaged O_3) calculated at 1-hour intervals, are also shown.

$$P(O_3) = k_1[NO][HO_2] + \Sigma\, k_i[NO][R_iO_2] - [O_3] \cdot \{k_3[OH]+k_4[HO_2]\} - k_5[O(^1D)][H_2O] \quad (2)$$

The symbol R_iO_2 stands for CH_3O_2, $C_2H_5O_2$, CH_3CO_3, $C_3H_7O_2$, $C_3H_6OHO_2$, or $C_2H_4OHO_2$, i.e., free radicals derived from OH oxidation of hydrocarbons. Integrating over the diurnal cycle and averaging over 24 hours gives a mean ozone production potential of -1.3 ppbv O_3/d for 9–10 ppbv O_3 at the equator. This is typical; with NO at <5 pptv, even assuming the maximum NMHC levels measured by *Atlas et al.* [this issue], $P(O_3)$ would be expected to be negative [*Liu et al.*, 1983; *Carroll et al.*, 1990]. Taking the lower hydrocarbon data of *Donahue and Prinn* [this issue] (50 pptv C_2H_4 and 55 pptv C_3H_6 compared to 420 pptv C_2H_4 and 150 pptv C_3H_6 measured by *Atlas et al.* [this issue]) makes little difference (<15%) in the O_3 production potential. This is because the predominant O_3 formation processes are NO reactions with CH_3O_2 and HO_2 rather than with R_iO_2. Ozone formation is slower, however, than loss of O_3 due to O_3 reaction with HO_2 and $O(^1D)$ reaction with H_2O.

The O_3 production potential is most sensitive to the level

of O_3 itself in this low NO, low NMHC environment. This can also be seen by looking at the OPP at three levels of O_3:

5°S (6 ppbv mean O_3) − 0.5 ppbv O_3/d

0° (10 ppbv mean O_3) − 1.3 ppbv O_3/d

10°N (20 ppbv mean O_3) − 2.3 ppbv O_3/d.

Because assumed NO and hydrocarbons are similar in the three cases, most differences in formation and loss processes are due to differences in HO_2 and $O(^1D)$ and vary directly with the concentration of O_3 or the rate of O_3 UV photodissociation. The predominant O_3 loss is due to $O(^1D)$ reaction with H_2O and this is greatest at 10°N. The reaction between O_3 and HO_x (HO_x = OH + HO_2), which is proportional to $(O_3)^2$, is the other O_3 loss process. Thus in a fairly narrow range of latitudes a three-fold variation in O_3 concentrations causes more than a factor of 4 variation in OPP. However, the photochemical lifetime of O_3, given by the ratio OPP/(mean O_3 concentration) does not vary much among these latitudes.

Ozone levels in the marine troposphere are determined by photochemical loss or formation, downward transport from the stratosphere, and long-range transport from regions of higher O_3. Isobaric trajectories of the air masses encountered by SAGA 3 showed that air near the surface and at 850 mbar (roughly at the trade wind inversion) was consistently 1 week or more removed from continental source regions which could export O_3 or O_3 precursors [*Johnson et al.*, this issue]. Thus it appears that downward transport and photochemical destruction are the most important factors in determining the O_3 levels observed on SAGA 3.

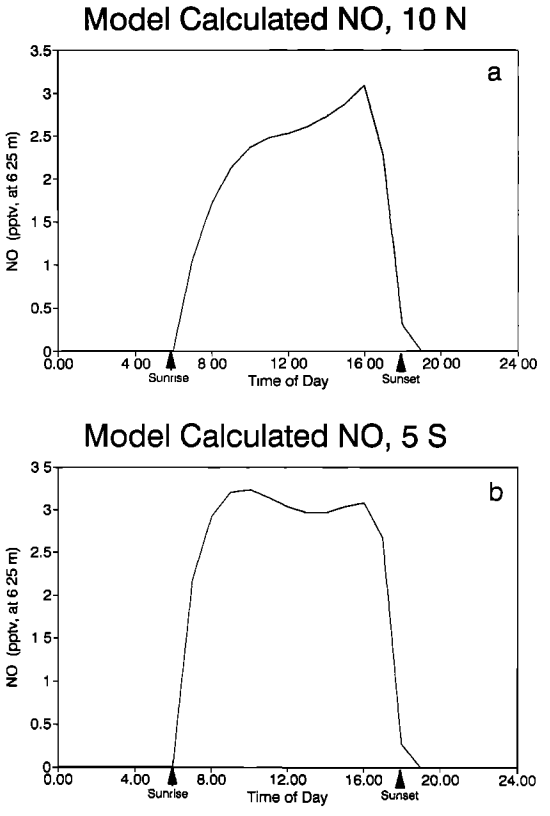

Fig. 7. Diurnal variation of NO mixing ratios, showing the difference in photochemical processes between (*a*) 10°N (mean O_3 = 20 ppbv) and (*b*) 5°S (mean O_3 = 6 ppbv). Observed mean daylight concentration is 2.9 ± 0.2 pptv [*Torres and Thompson*, this issue].

5.2. *NO and Alkyl Nitrates*

The low levels of nitric oxide measured on SAGA 3 with the NASA/Wallops Flight Facility instrument are described by *Torres and Thompson* [this issue]. The mean daytime value is 2.9 ± 0.2 pptv, which compares well with the shipboard equatorial Pacific NO measurements of *McFarland et al.* [1979] on *Knorr 73/7*. In fact, on SAGA 3 the mean concentration of daytime NO within 5° of the equator is 4 pptv, identical to the *McFarland et al.* [1979] values in the equatorial upwelling region. On SAGA 3 at latitudes greater than 5°, NO concentrations averaged 2 pptv [*Torres and Thompson*, this issue]. Nitric oxide concentrations on SAGA 3, as on *Knorr 73/7*, were undetectably low at night. Zafiriou and coworkers [*Zafiriou et al.*, 1980; *Zafiriou and McFarland*, 1981] have suggested that a major source of boundary layer NO in the equatorial Pacific is a weak oceanic outgassing of dissolved NO formed from photodissociation of the nitrite (NO_2^-) radical [*Treinin and Hayon*, 1970; *Bonneau*, 1987]:

$$NO_2^- + H_2O + h\nu \rightarrow NO + OH + OH^-$$

The nitrite is presumed to be of photochemical origin. Although nitrite was not measured on SAGA 3, concentrations of seawater chlorophyll and nitrate maximized near the equator and sea surface temperature was at a minimum, indicating upwelling [*Johnson et al.*, this issue]. In general, in non-El Niño years, a broad nitrite maximum associated with upwelling can be assumed for the region traversed on SAGA 3 (O. C. Zafiriou, personal communication, 1992).

Several organobromine and alkyl nitrate constituents also showed equatorial maxima on SAGA 3 [*Atlas et al.*, this issue]. Model simulations of NO diurnal behavior, calculated assuming a daytime flux of 1.1×10^8 cm^{-2} s^{-1}, give a noontime NO mixing ratio of 2.6 pptv. Thus the 4 pptv equatorial concentrations would be supported by $\sim 1.5 \times 10^8$ cm^{-2} s^{-1}, in reasonable agreement with the flux estimated by *Zafiriou and McFarland* [1981] from NO supersaturation in seawater on the 1978 *Knorr 73/7* cruise.

Figure 7 shows the diurnal behavior of NO at 5°S (Figure 7*a*) and 10°N (Figure 7*b*). In both cases mean daytime concentrations are 3–3.5 pptv, but the early morning maximum NO concentration at 5°S (mean O_3 = 6 ppbv) does not appear in the 10°N case. This is because higher levels of O_3 at 10°N convert more NO to NO_2 and the O_3 maximum occurs in the early morning. For 0800 LT the NO mixing ratio is suppressed at 10°N and the ratio NO_2/NO is 2.7 for 10°N and 1.1 at 5°S. The model is used to evaluate the diurnal variation in NO_2/NO, the so-called photostationary state ratio [*Stedman and Jackson*, 1975], although no NO_x or NO_2 measurements were made on SAGA 3. The NO mixing ratios follow those observed fairly closely [*Torres and Thompson*, this issue] and NO_2 is computed from the model. The model also computes an expression proposed as an approximation to the photostationary state:

$$NO_2/NO = \text{"photostationary state (PSS)"}$$

$$= (J_3)^{-1} \{k_6[O_3] + k_{25}[HO_2] + \Sigma\, k_i[NO][R_iO_2]\} \quad (3)$$

where the free radicals in (3) are the same as in (2) and J_3 is the photodissociation rate for NO_2. If the cycling between NO and NO_2 were only mediated by O_3, the NO_2/NO ratio would equal $k_6[O_3]/J_3$, but the model shows that the latter expression is only 0.4–0.5 during midday [*Torres and Thompson*, this issue]. *Chameides et al.* [1990] analyzed remote Pacific boundary layer measurements of NO, NO_2, and O_3 from NASA/GTE/CITE 2 (Global Tropospheric Chemistry/Chemical Intercomparison and Test Evaluation) aircraft experiments to show that in the nonpolluted Pacific boundary layer and free troposphere, photostationary state ratios of 1.2–2 are typical and that (3) is well-obeyed. SAGA 3 values for the photostationary state at noon, deduced from model-calculated NO and NO_2, are within the same range and show variation with NO_x and O_3 levels:

Latitude, mean O_3	NO_2/NO
5°S (6 ppbv)	1.2
0° (10 ppbv)	1.45
10N (20 ppbv)	2.1

These compare to an NO_2/NO ratio of ~4 when diurnally averaged mixing ratios are used (Table 4). Although agreement with the CITE 2 measurements is validation of the model to some degree, the photostationary state ratios here are based on model-calculated values that closely simulate O_3 and NO, not measurements of NO, NO_2, and O_3.

Total alkyl nitrate concentrations on SAGA 3 ranged from 5 to 15 pptv for a half-dozen nitrates [*Atlas et al.*, this issue]. Mean hydrocarbon and NO mixing ratios (Table 4) correspond to a sum of the three alkyl nitrates equal to 0.5 pptv, which is much less than observed. Photochemical model calculations of mixing ratios at the 6.25-m level for three alkyl nitrates (ethyl nitrate, 1-propyl, and 2-propyl nitrate) are parameterized [*Atlas et al.*, this issue]. Maximum and minimum formation rates are based on alkane mixing ratios reported by *Atlas et al.* [this issue] and *Donahue and Prinn* [this issue] and on NO mixing ratios at 1 or 2 pptv. The computed sum of ethyl, 1-propyl, and 2-propyl nitrate ranges from 0.2 to 2.5 pptv, much lower than the observed total of 5–15 pptv. The difference between computed and observed alkyl nitrate levels indicates long-range transport of alkyl nitrates from continental regions where concentrations of 100–200 pptv are expected [*Atherton*, 1989; *Buhr et al.*, 1990; *Atlas et al.*, 1992]. With photochemical lifetimes of 2–3 weeks, residual concentrations of several pptv could persist after the 7- to 10-day trip from land to the SAGA 3 sampling area (see *Johnson et al.* [this issue] for SAGA 3 trajectories).

Neither in situ photochemical production nor long-range transport can account for apparent equatorial maxima in ethyl nitrate (5 pptv) and 2-propyl nitrate (8 pptv) from the SAGA 3 samples. *Atlas et al.* [this issue] also found equatorial maxima in bromoform and $CHClBr_2$ concentration levels, species that are usually interpreted as markers for biological activity. If an oceanic source of alkyl nitrate is responsible for the equatorial maximum, a flux of 7×10^7 cm^{-2} s^{-1} would be required to maintain 8 pptv 2-propyl nitrate against photolysis and reaction with OH.

5.3. *Other Oxidants: Peroxides and OH*

The peroxide measurements appear to be the first in the equatorial Pacific boundary layer. The diurnal behavior of the peroxides measured on SAGA 3, H_2O_2, and the soluble organoperoxides (ROOH), is shown in Figure 8 along with mixing ratios at the 6.25-m level computed from the photochemical model (ROOH = CH_3OOH + C_2H_5OOH). Mean H_2O_2 on SAGA 3 was 600 pptv (± 30%) and ROOH was 650 pptv (± 20%) (Table 4). The model ascribes more than 95% of the ROOH to CH_3OOH, a byproduct of the oxidation of CH_4 (Table 3), with the remainder from ethylhydrogen peroxide, C_2H_5OOH. Ethylhydrogen peroxide results from OH oxidation of C_2H_6 (with mean mixing ratio ~800 pptv on SAGA 3 [*Atlas et al.*, this issue; *Donahue and Prinn*, this issue]).

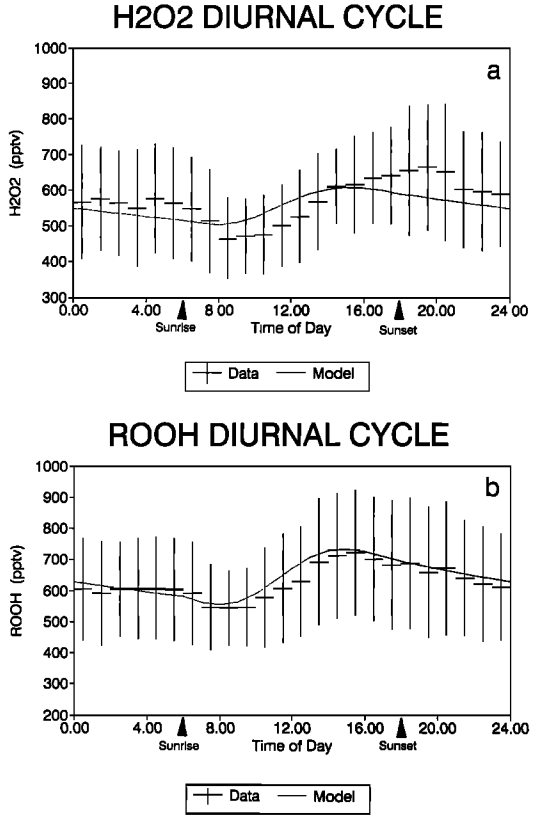

Fig. 8. Diurnal variation of H_2O_2 and soluble organic peroxides (ROOH) mixing ratios and model calculated H_2O_2 and ROOH (= CH_3OOH + C_2H_5OOH) at 6.25 m (close to ship height). Hourly averages of all peroxide observations are plotted with 1σ standard deviation at 95% confidence limits. Mean daylight concentrations are 0.55 ± 0.15 ppbv for H_2O_2 and 0.65 ± 0.18 ppbv for ROOH. Model calculations show ROOH consisting of ≥95% CH_3OOH. Time of day is Hawaiian time (local ship time for most of cruise); model conditions are for March 1, 1990.

The diurnal variations for peroxides derive from a buildup of free radicals (e.g., CH_3O_2 and HO_2) during the day, balanced by OH oxidation and photolysis. The SAGA 3 diel pattern (maximum mixing ratio 50% higher than the minimum) is nearly identical to that reported recently by *Ayers et al.* [1992] for peroxides measured in the unpolluted marine boundary layer at the Cape Grim, Tasmania, monitoring site (41°S). At Cape Grim the mean peroxide concentration, presumed to consist mostly of H_2O_2 and a small amount of CH_3OOH, is ~800 pptv. The model calculation includes surface deposition and a first-order removal term for H_2O_2 to represent precipitation (or aerosol) scavenging. The scavenging coefficient is not varied over a diurnal cycle and thus may not be appropriate for SAGA 3 conditions. On nearly

TABLE 5. OH and HO_2 Radical Concentrations for SAGA 3

Latitude	Mixing Ratio, 24-hour Mean			
	O_3, ppbv	CO, ppbv	OH, $\times 10^5$ cm^{-3}	HO_2, pptv
5°S	6.0	53	7.1	4.2
0°	9.3	75	8.9	5.2
10°N	20	90	12	6.1

Model results with above-tropospheric O_3 = 216 DU, solar conditions of March 1, 1990; mixing ratios for NO_x/NMHC/DMS as in Table 4.

every day there was a brief shower at or near the vicinity of the *Korolev* and a periodic scavenging loss might be more realistic. There was not a clear pattern in precipitation on the cruise. There was also a slight diurnal cycle in relative humidity not accounted for in the model (minimum in late afternoon). Nonetheless, the model simulation of the diurnal cycle is satisfactory, with agreement better for ROOH (Figure 8*b*) than for H_2O_2 (Figure 8*a*). With lower solubility compared to H_2O_2, the organic peroxides are less subject to scavenging assumptions.

Table 5 shows that the diurnally averaged OH for mean surface O_3 of 9.3 ppbv is 8.9 $\times$ 10^5 cm^{-3}. The hydroxyl radical is produced by photolysis of O_3 followed by attack of the energetic $O(^1D)$ on H_2O:

$$O_3 + h\nu \rightarrow O(^1D) + O_2$$

$$O(^1D) + H_2O \rightarrow OH + OH.$$

In model simulations with "low" (Table 4) hydrocarbons the main sinks for OH are reaction with CH_4 (25%) and CO (37%). Reactions with H_2CO, H_2O_2, and CH_3OOH combined account for 17% of OH removal and NMHC account for 3.5% of OH loss. Nonmethane hydrocarbons contribute significantly to OH loss (17%) if "high" NMHC concentrations (Table 4) are assumed. Reaction with DMS represents 4–5% of OH loss in the boundary layer. These assessments of OH chemistry are similar to those of *Donahue and Prinn* [this issue], who report mean OH to be 6 $\times$ 10^5 cm^{-3}. *Yvon et al.* [this issue], using a box model with no NMHC chemistry, compute a diurnally averaged OH number density of 7.9 $\times$ 10^5 cm^{-3} for surface O_3 equal to 9 ppbv with assumptions the same as ours for H_2O, overhead O_3, temperature, and solar zenith angle. This is ~11% lower than the value from the one-dimensional model.

5.4. *Sulfur Species and CO*

Table 6 gives the model-derived fluxes of several species measured on SAGA 3 that are assumed to have an oceanic source. *Bates et al.* [this issue] measured both atmospheric and dissolved CO on SAGA 3 and observed a distinct diurnal variation (±25% about the mean) in the latter. Assuming the observed wind velocities and the relationship of *Liss and Merlivat* [1986] to derive the sea-to-air transfer velocity, *Bates et al.* [this issue] calculate that the sea-to-air flux due to oceanic CO supersaturation is ~3 $\times$ 10^9 cm^{-2} s^{-1}. This is only 2.5% of the model flux required to balance CO reaction with OH (Table 6). In other words the local CO source supports little of the atmospheric CO burden in the equatorial Pacific. Indeed, the diurnal variation in atmospheric CO due to seawater supersaturation is only ~1 part in 10^8 of the observed level [*Johnson et al.*, 1991]. On a global basis the oceanic source of CO is estimated to be 5% or less [*Logan et al.*, 1981].

TABLE 6. SAGA 3 Mixing Ratios and Corresponding Fluxes From One-Dimensional Model

Species	Model, 24-hour Mean Mixing Ratio, 6.25 m	Flux,* molecules cm^{-2} s^{-1}
NO	1.3 pptv	8.2 $\times$ 10^7
CO	75 ppbv	1.2 $\times$ 10^{11}
DMS	380 pptv	7.6 $\times$ 10^9
H_2S	2.8 pptv	5.3 $\times$ 10^7
CS_2	3.6 pptv	5.8 $\times$ 10^7
C_2H_4	50–420 pptv	1.3–11 $\times$ 10^9
C_2H_6	790 pptv	2.0 $\times$ 10^9
C_3H_6	55–150 pptv	2.4–6.5 $\times$ 10^9
C_3H_8	64–85 pptv	4.8–6.5 $\times$ 10^8

Same conditions as for Table 4.
*Diurnally averaged flux; diurnally averaged OH at 6.25 m = (0.86–0.89) $\times$ 10^6 cm^{-3}.

Figure 9 shows the calculated diurnal variations in atmospheric CO mixing ratio for equatorial conditions. The observed diurnal cycle, approximately 1 ppbv between maximum and minimum values, is slightly larger than the calculated variation (0.6 ppbv) which is due to photochemical reaction with OH. On other Pacific cruises (e.g., RITS 88 and 89), tropical data for atmospheric CO mixing ratios show a diurnal variation of ~2 ppbv [*Johnson et al.*, 1991].

Agreement between model calculations and observations for DMS, SO_2, and H_2S is good (Table 4). Of course, this is forced in the model by selecting a sea-to-air flux that reproduces the shipboard measurement. A test of whether the model OH concentrations are "correct" is to compare the model-deduced DMS lifetime (and sea-to-air DMS flux) to the flux derived from the seawater supersaturation of the dissolved trace gas. The model-deduced flux is given by

$$\text{flux(DMS)}_{\text{model}} - [\text{DMS}](k_{77}[\text{OH}] + k_{63}[\text{NO}_3]) = 0$$

where the concentrations are diurnally averaged values at 0 km computed by the model and the lifetime is given by the factor multiplying (DMS). For typical SAGA 3 conditions (10 ppbv O_3 and diurnally averaged OH equal to 9 $\times$ 10^5 cm^{-3}), less than 1% of DMS reacts with NO_3, so self-

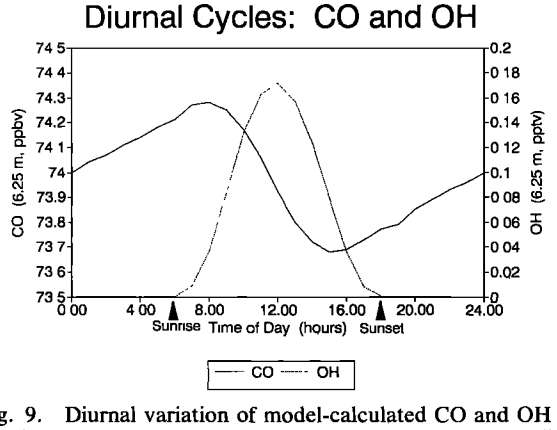

Fig. 9. Diurnal variation of model-calculated CO and OH mixing ratios at 6.25 m for equatorial conditions. Observed diurnal variation in shipboard CO measurements follows the simulation but is slightly larger.

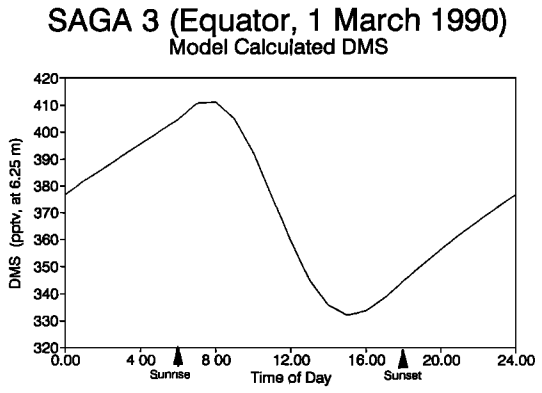

Fig. 10. Diurnal DMS behavior computed by the photochemical model constrained by the SAGA 3 trace gas mixing ratios given in Table 4.

consistency between the model and the "measured" fluxes is a check on OH. The flux deduced from atmospheric DMS, $\text{flux(DMS)}_{\text{model}}$, 7.6×10^9 cm^{-2} s^{-1} (Table 6), is ~50% higher than that derived from SAGA 3 seawater DMS concentration and surface winds: $\text{flux(DMS)}_{\text{seawater}} = 5.4 \times 10^9$ cm^{-2} s^{-1} [*Bates et al.*, this issue]. The combined uncertainties in the OH concentration and its reaction rate with DMS are at least 25%. Fluxes derived from the seawater DMS would be nearly a factor of 2 higher if a different relationship between the surface winds and the sea-to-air transfer rate were used [*Bates et al.*, this issue; *Wanninkhof*, 1992]. Thus agreement between the DMS flux estimated from the model falls midway between the two seawater-DMS-based estimates and is within the uncertainty range for each method. However, a discrepancy between an atmospheric DMS-based flux (equivalent to our $\text{flux(DMS)}_{\text{model}}$) and a DMS flux from seawater DMS concentrations, $\text{flux(DMS)}_{\text{seawater}}$, is implied by observations in the tropical Atlantic (E. S. Saltzman et al., Diurnal variations in atmospheric sulfur gases over the western equatorial Atlantic Ocean, submitted to *Journal of Geophysical Research*, 1993). For that region the atmospheric-based DMS flux may be larger than $\text{flux(DMS)}_{\text{seawater}}$ by up to a factor of 2. Several cruises since SAGA 3 also show atmospheric DMS concentrations higher than expected from equilibrium with seawater DMS (T. S. Bates, personal communication, 1992).

Model results can be used to estimate the photochemical lifetime of DMS in two ways. First, using the model-derived flux (7.6×10^9 cm^{-2} s^{-1}), with 300 pptv mean DMS in the mixed layer of depth, H, 1.5 km [*Johnson et al.*, this issue], the lifetime can be estimated from

$$[\text{DMS (cm}^{-3})] \times \text{H/flux} = 1.44 \times 10^5 \, s \text{ (40.1 hour)}.$$

Looking at Figure 10 the diurnal variation in DMS shows a 20% loss in 7–8 hours (from 0700 to 1400), suggesting a lifetime of 35–40 hours. The latter estimate cannot be verified with SAGA 3 observations because diurnal variation in atmospheric DMS was not consistently monitored. *Huebert et al.* [this issue] estimate DMS lifetime by the atmospheric burden/flux approach to be 3 days. Observations of DMS diurnal variation and seawater concentrations from other cruises are consistent with lifetimes <1 day [*Bates et al.*, 1990; *Cooper and Saltzman*, 1991]. Our estimates are intermediate in this range and point toward shorter lifetimes (higher OH levels with a given sea-to-air flux) as more realistic.

6. Summary and Conclusions

Measurements of photochemically reactive trace gases made during the SAGA 3 oceanographic cruise offered an opportunity to test present photochemical theory of ozone and C-, N-, and S-containing gases in a nonpolluted marine environment. Major findings are as follows:

1. The low O_3, low NO_x, low hydrocarbon picture of equatorial Pacific trace gases deduced from a few species measured on previous cruises was confirmed with a more comprehensive set of observations, although O_3 levels were not as low as on some previous cruises. A one-dimensional photochemical model using observed mixing ratios of O_3/NO/CO/CH_4/NMHC reproduces the observed O_3 pattern of destruction during daytime and a maximum near sunrise. That total O_3 was very low (220–260 DU column abundance) throughout the SAGA 3 study region was confirmed with an on-board UV instrument which agreed with total O_3 from Nimbus 7 TOMS satellite observations to within 10%.

2. Interpretation of the SAGA 3 data set with a photochemical model gives self-consistent values of reactive gases besides O_3 measured on the cruise: DMS, CO, CH_4, NMHC, NO, H_2S. Analysis of O_3-CO-NO-NMHC-CH_4 chemistry at concentrations typical at the equator shows a destruction rate of 1.2 ppbv O_3/d when mean O_3 is ~10 ppbv (an 8-day photochemical lifetime for O_3). The corresponding photostationary ratio, NO_2/NO, based on measured O_3 and NO and model-calculated NO_2, is 1.4–1.5, in agreement with current photochemical theory. This ratio is similar to actual measurements of the NO_2/NO ratio on GTE/CITE 2 flights in the remote Pacific [*Carroll et al.*, 1990; *Chameides et al.*, 1990].

3. Trace gas measurements constrain model-calculated OH to 9×10^5 cm^{-3}, for a range of O_3 mixing ratios from 6 to 20 ppbv, respectively. Our values are somewhat higher than those computed by two box models used to simulate SAGA 3 data. The diurnal variation of atmospheric CO, which is due to reaction with OH, is small (~1 ppbv). The diurnal patterns of H_2O_2 and ROOH observed on SAGA 3 are reasonably well reproduced by the model. The peroxides are an important component of the oxidizing capacity of the marine environment, but they do not provide an important constraint to model calculation of OH for SAGA 3.

4. To the extent possible (i.e., given uncertainties in measured trace gas concentrations and computed sea-to-air transfer rates) the lifetime calculation of DMS (i.e., model calculation of OH) was validated by SAGA 3. It is difficult to reduce the discrepancy between the sea-to-air DMS flux deduced from the model and from measurement of dissolved DMS on SAGA 3 (~50%) with current theory and experimental technique.

5. Several trace gases measured on SAGA 3 (NO, ethyl and 2-propyl nitrate, bromoform, and $CHClBr_2$) showed maximum concentrations at the equator, suggestive of photochemical or biological sources of these gases.

Although the comprehensive set of observations made on SAGA 3 achieved most of the photochemical objectives of the cruise, several issues call for further study and alternative experimental design. First, the data set collected was not Lagrangian and assumed boundary conditions are only

approximately correct for the individual air parcels sampled over the course of the cruise. In the future we aim for combined ship-aircraft experiments to better characterize regional chemistry, meteorology, and to track air masses. More definitive analysis of O_3 chemistry and dynamics, for example, awaits such an experiment.

The goal of constraining model calculation of OH on SAGA 3 was quite successful, but the discrepancy among three models shows the limitations of not having a direct OH measurement. The model OH may be responsible for some of the discrepancy between a DMS flux derived from a photochemical model (constrained by measurement of atmospheric DMS concentration) and one derived from seawater DMS measurements. However, analysis of atmospheric and seawater DMS measurements suggests that this is a more complex problem than uncertainty in OH [*Bates et al.*, this issue; *Huebert et al.*, this issue]. Besides OH there is a more general lack of closure in the chemical data set. Odd nitrogen species measurements, in particular, were not complete on SAGA 3; total reactive odd nitrogen (NO_y), NO_2, PAN, and HNO_3 are needed in addition to NO and the alkyl nitrates. Finally, direct measurements of the O_3 and NO_2 photodissociation rates would put constraints on both NO_x and HO_x.

Acknowledgments. AMT thanks the Goddard Director's Discretionary Fund, the NASA Tropospheric Chemistry Program, and a NASA EOS Interdisciplinary Project (joint with Woods Hole Oceanographic) for support. JEJ, TSB, and KCK acknowledge support from the RITS and Marine Sulfur and Climate Change components of the NOAA Climate and Global Change Program. BGH and BM thank G. Kok and V. Mohnen for graciously lending peroxide instrumentation and NSF for making their participation possible with supplementary support to ATM 87-02563. We are grateful to chief scientist Valentin M. Koropalov (IAG, Moscow), Captain Gennady N. Chubakov, and the crew of the R/V *Akademik Korolev* for working hard to ensure the success of SAGA 3 photochemical objectives. We appreciate logistical support from Elmer Robinson and Judy Pereira at the NOAA/CMDL office in Hilo. Thanks to Goddard colleagues T. L. Kuscera (Applied Research Corp.) for programing assistance and P. A. Newman and D. P. McNamara for retrieving TOMS satellite data. We thank O. C. Zafiriou (Woods Hole Oceanographic) for comments on the manuscript.

REFERENCES

Atherton, C. S., Organic nitrates in remote marine environment: Evidence for long-range transport, *Geophys. Res. Lett.*, *16*, 1289–1292, 1989.

Atlas, E., S. M. Schauffler, J. T. Merrill, C. J. Hahn, B. Ridley, J. Walega, J. Greenberg, L. Heidt, and P. Zimmerman, Alkyl nitrate and selected halocarbon measurements at Mauna Loa Observatory, Hawaii, *J. Geophys. Res.*, *97*, 10,331–10,348, 1992.

Atlas, E., W. Pollock, J. Greenberg, L. Heidt, and A. Thompson, Alkyl nitrates, nonmethane hydrocarbons, and halocarbon gases over the equatorial Pacific Ocean during SAGA 3, *J. Geophys. Res.*, this issue.

Ayers, G. P., S. A. Penkett, R. W. Gillett, B. Bandy, I. E. Galbally, C. P. Meyer, C. M. Ellsworth, S. T. Bentley, and B. W. Forgan, Evidence for photochemical control of ozone concentrations in unpolluted marine air, *Nature*, *360*, 446–448, 1992.

Bates, T. S., K. C. Kelly, and J. E. Johnson, Concentrations and fluxes of dissolved biogenic gases (DMS, CH_4, CO, CO_2) in the equatorial Pacific during the SAGA 3 experiment, *J. Geophys. Res.*, this issue.

Bonneau, R., Wavelength dependence of quantum yield of OH radical formation from photolysis of nitrite ion in water, *Photochem. Photobiol.*, *45*, 723–727, 1987.

Buhr, M. P., D. D. Parrish, R. B. Norton, F. C. Fehsenfeld, R. E. Sievers, and J. M. Roberts, Contribution of organic nitrates to the total reactive nitrogen budget at a rural eastern U.S. site, *J. Geophys. Res.*, *95*, 9809–9816, 1990.

Carroll, M. A., et al., Aircraft measurements of NO_x over the eastern Pacific and continental United States and implications for ozone production, *J. Geophys. Res.*, *95*, 10,205–10,233, 1990.

Chameides, W. L., et al., Observed and model-calculated NO_2/NO ratios in tropospheric air sampled during the NASA GTE/CITE 2 field study, *J. Geophys. Res.*, *95*, 10,235–10,247, 1990.

Cooper, D. W., and E. S. Saltzman, Measurements of atmospheric dimethylsulfide and carbon disulfide in the western Atlantic boundary layer, *J. Atmos. Chem.*, *12*, 153–168, 1991.

Donahue, N. M., and R. G. Prinn, In situ nonmethane hydrocarbon measurements on SAGA 3, *J. Geophys. Res.*, this issue.

Gushchin, G. P., K. I. Romashkina, and A. M. Shalamyanskiy, (in Russian), *State Hydrometeorol. Rep. 357*, 106–122, 1976.

Huebert, B. J., S. Howell, P. Laj, J. E. Johnson, T. S. Bates, P. K. Quinn, V. Yegorov, A. D. Clarke, and J. N. Porter, Observations of the atmospheric sulfur cycle on SAGA 3, *J. Geophys. Res.*, this issue.

Johnson, J. E., R. H. Gammon, J. Larsen, T. S. Bates, S. J. Oltmans, and J. C. Farmer, Ozone in the marine boundary layer over the Pacific and Indian oceans: Latitudinal gradients and diurnal cycles, *J. Geophys. Res.*, *95*, 11,847–11,856, 1990.

Johnson, J. E., K. C. Kelly, and A. M. Thompson, The diurnal behavior of atmospheric carbon monoxide in the marine boundary layer: Observations and theory, *Eos Trans. AGU*, *72*(44), Fall Meeting suppl., 106, 1991.

Johnson, J. E., V. M. Koropalov, K. E. Pickering, A. M. Thompson, and N. Bond, SAGA-3 experiment: Overview and meteorological and oceanographic conditions, *J. Geophys. Res.*, this issue.

Liss, P. S., and L. Merlivat, Air-sea gas exchange rates: Introduction and synthesis in *The Role of Air-sea Exchange in Geochemical Cycling*, edited by P. Buat-Menard, pp. 113–127, D. Reidel, Norwell, Mass., 1986.

Liu, S. C., M. McFarland, D. Kley, O. Zafiriou, and B. Huebert, Tropospheric NO_x and O_3 budgets in the equatorial Pacific, *J. Geophys. Res.*, *88*, 1360–1368, 1983.

Logan, J. A., M. J. Prather, S. C. Wofsy, and M. B. McElroy, Tropospheric chemistry: A global perspective, *J. Geophys. Res.*, *86*, 7210–7254, 1981.

Lowe, D., and U. Schmidt, Formaldehyde in the clean troposphere, in *Proceedings of the 2nd Symposium on Composition of the Nonurban Troposphere*, pp. 288–291, American Meteorological Society, Boston, Mass., 1982.

McFarland, M., D. Kley, J. W. Drummond, A. L. Schmeltekopf, and R. H. Winkler, Nitric oxide measurements in the equatorial Pacific region, *Geophys. Res. Lett.*, *6*, 605–608, 1979.

NASA Jet Propulsion Laboratory, Chemical kinetics and photochemical data for use in stratosphere modeling, in Evaluation 9, *JPL Publ. 90-1*, 1990.

Oltmans, S. J., and W. D. Komhyr, Surface ozone distributions and variations from 1973 to 1984 measurements at the NOAA Geophysical Monitoring for Climatic Change Baseline Observatories, *J. Geophys. Res.*, *91*, 5229–5236, 1986.

Paluch, I. R., D. H. Lenschow, J. G. Hudson, and R. Pearson, Jr., Transport and mixing processes in the lower troposphere over the ocean, *J. Geophys. Res.*, *97*, 7527–7542, 1992.

Piotrowicz, S. R., D. A. Boran, and C. K. Fischer, Ozone in the boundary layer of the equatorial Pacific Ocean, *J. Geophys. Res.*, *91*, 13,113–13,119, 1986.

Piotrowicz, S. R., H. F. Bezdek, G. R. Harvey, M. Springer-Young, and K. J. Hanson, On the ozone minimum over the equatorial Pacific Ocean, *J. Geophys. Res.*, *96*, 18,679–18,687, 1991.

Platt, U., J. Rudolph, T. Brauers, and G. W. Harris, Atmospheric measurements during Polarstern Cruise ANT VII/1, 54°N to 32°S: An overview, *J. Atmos. Chem.*, *15*, 203–214, 1992.

Roberts, J. M., The atmospheric chemistry of organic nitrates, *Atmos. Environ.*, *24*(A), 243–287, 1990.

Routhier, F., R. Dennett, D. D. Davis, A. Wartburg, P. Haagenson, and A. C. Delany, Free tropospheric and boundary layer airborne measurements of ozone over the latitude of range of 58°S and 70°N, *J. Geophys. Res.*, *85*, 7307–7321, 1980.

Rudolph, J., and F. J. Johnen, Measurements of light atmospheric hydrocarbons over the Atlantic in regions of low biological activity, *J. Geophys. Res.*, *95*, 20,583–20,591, 1990.

Shiotani, M., Annual, quasi-biennial and El Nino-Southern Oscillation (ENSO) time scale variations in equatorial total ozone, *J. Geophys. Res.*, *97*, 7625–7634, 1992.

Stedman, D. H., and J. O. Jackson, The photostationary state in photochemical smog, *Int. J. Chem. Kinet.*, *1*, 493–501, 1975.

Thompson, A. M., and R. J. Cicerone, Clouds and wet removal as causes of variability in the trace gas composition of the marine troposphere, *J. Geophys. Res.*, *87*, 8811–8826, 1982.

Thompson, A. M., and D. H. Lenschow, Mean profiles of reactive trace gases in the unpolluted marine surface layer, *J. Geophys. Res.*, *89*, 4788–4796, 1984.

Thompson, A. M., and R. W. Stewart, Effects of chemical kinetics uncertainties on calculated constituents in a tropospheric photochemical model, *J. Geophys. Res.*, *96*, 13,089–13,108, 1991.

Thompson, A. M., W. E. Esaias, and R. L. Iverson, Two approaches to determining the sea-to-air flux of dimethyl sulfide: Satellite ocean color and a photochemical model with atmospheric measurements, *J. Geophys. Res.*, *95*, 20,551–20,558, 1990.

Torres, A. L., and A. M. Thompson, Nitric oxide in the equatorial Pacific boundary layer: SAGA 3 measurements, *J. Geophys. Res.*, this issue.

Treinin, A., and E. Hayon, Absorption spectra and reaction kinetics of NO_2, N_2O_3, and N_2O_4 in aqueous solution, *J. Am. Chem. Soc.*, *92*, 5821–5828, 1970.

Wanninkhof, R., Relationship between wind speed and gas exchange over the ocean, *J. Geophys. Res.*, *97*, 7373–7382, 1992.

Yegorov, V., Spatial distribution of ozone, sulfur dioxide and sulphates in the marine boundary layer of the atmosphere (abstract), *Eos, Trans. AGU*, *71*, 1230, 1990.

Yvon, S., D. J. Cooper, V. M. Koropalov, and E. S. Saltzman, Atmospheric hydrogen sulfide over the equatorial Pacific (SAGA 3), *J. Geophys. Res.*, this issue.

Zafiriou, O. C., and M. McFarland, Nitric oxide from nitrite photolysis in the central equatorial Pacific, *J. Geophys. Res.*, *86*, 3173–3182, 1981.

Zafiriou, O. C., M. McFarland, and R. H. Bromund, Nitric oxide in seawater, *Science*, *207*, 637–639, 1980.

E. Atlas and J. P. Greenberg, National Center for Atmospheric Research, P.O. Box 3000, Boulder, CO 80307.

T. S. Bates, J. E. Johnson, and K. C. Kelly, NOAA Pacific Marine Environmental Laboratory, 7600 Sand Point Way NE, Seattle, WA 98115.

N. M. Donahue, Harvard University, 40 Oxford Street, Cambridge, MA 02138.

B. G. Heikes, Graduate School of Oceanography, University of Rhode Island, Narragansett Bay Campus, Kingston, RI 02882.

B. W. Mosher, Eos Science and Engineering Building, University of New Hampshire, Durham, NH 03824.

E. S. Saltzman and S. A. Yvon, Rosenstiel School of Marine and Atmospheric Science, University of Miami, Miami, FL 33149.

A. A. Shashkov, Main Geophysical Observatory, St. Petersburg, Russia.

A. M. Thompson, NASA Goddard Space Flight Center, Mail Code 916, Greenbelt, MD 20771.

A. L. Torres, NASA Goddard SFC, Wallops Flight Facility, Code 972, Wallops Island, VA 23337.

V. I. Yegorov, Institute of Applied Physics, Laboratory for Atmospheric Monitoring, Moscow, Russia.

(Received July 16, 1992;
revised January 25, 1993;
accepted January 26, 1993.)